Journal of Mathematical Chemistry (2025) 63:1566–1587
https://doi.org/10.1007/s10910-025-01731-y

ORIGINAL PAPER

To a mechanical model of synthetic catch-bonds

Wolfgang Quapp[1] · **Josep Maria Bofill**[2,3] · **Kerim C. Dansuk**[4] · **Sinan Keten**[5,6]

Received: 16 January 2025 / Accepted: 26 April 2025 / Published online: 8 May 2025

Abstract

Abstract We support a preliminary determination of the catch-bond character of a mechanical–chemical toy model using a tweezers construction with some modifications. We discuss a theoretical analysis of the problem using Newton trajectories. We propose a two-dimensional potential energy surfaces for this model. We discuss the slip, ideal and catch-bonds for this model using the previous potential parts of Dansuk and Keten (Matter 1:911, 2019). Chemical examples of the ansatz are allosteric reactions, especially FimH proteins. We note again that Newton trajectories provide the theoretical background of mechanochemistry. Construction of a potential energy surface and use of Newton trajectories by Wolfram Mathematica. Calculation of real catch bond behavior. We get for a tweezers model the catch bond behavior.

✉ Wolfgang Quapp
quapp@math.uni-leipzig.de

Josep Maria Bofill
jmbofill@ub.edu

Kerim C. Dansuk
kerimcan.dansuk@bogazici.edu.tr

Sinan Keten
s-keten@northwestern.edu

1 Mathematics, Universität Leipzig, Augustus-Platz, PF 100920, 04009 Leipzig, Germany

2 Departament de Química Inorgànica i Orgànica, Secció de Química Orgànica, Universitat de Barcelona, Martí i Franquès 1, 08028 Barcelona, Spain

3 Institut de Química Teòrica i Computacional (IQTCUB), Universitat de Barcelona, Martí i Franquès 1, 08028 Barcelona, Spain

4 Mechanical Engineering Department, Boğaziçi University, Bebek, 34342 Istanbul, Turkey

5 Department of Mechanical Engineering, Northwestern University, 2145 Sheridan Road, Evanston, IL 60208, USA

6 Department of Civil and Environmental Engineering, Northwestern University, 2145 Sheridan Road, Evanston, IL 60208, USA

Graphical abstract

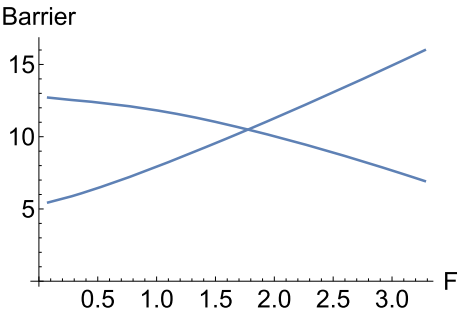

Two barriers under external force, F. The catch-bond barrier increases.

Keywords Mechanochemistry · Slip bond · Ideal bond · Catch-bond character · Tweezers model for FimH · 2D potential model · Newton trajectories

Mathematics Subject Classification 35A09 · 35A30 · 35B32 · 53A07 · 70G45

1 Introduction

This paper serves as a positive comment on the preliminary finding of the catch-bond character of a mechanical–chemical model using a tweezers construction. It was proposed in Matter 2019 [1]. A statistical analysis of the lifetime curves for a varity of parameters where reported for a mechanical analog of catch bonds. Here we present the result of the application of the fundamental theory of Newton trajectories (NT) for the solution of mechanochemical excitations of molecules [2, 3], especially for the application to catch-bonds [4]. The prerequisite for any application of NTs is the construction of a model of the potential energy surface (PES) of the system being treated. We will do this.

Catch bonds were first discovered 35 years ago [5], and have been observed in many biochemical molecules [6, 7]. The dissociation rate decreases as a result of the deformation of the molecule. Some of the aothors have recently reported [4] two proposed suitable free energy surfaces to model catch-bond behaviour [8, 9], as well as some other 2D models. Here we discuss the combination of parts of the Dansuk and Keten model [1]. In contrast to catch-bonds, there are typical bonds that weaken under a pulling force, called slip bonds. Between these two extremes are the ideal bonds, for which we are proposing an example for the first time below.

We are convinced that the theory of Newton trajectories (NT) [2, 3] is a tool for rationalizing the biochemical phenomena of slip- and catch-bonds. We consider that under an external force, one has to take into account the mechanochemical potential

$$V_f(\mathbf{x}) = V_o(\mathbf{x}) - F\,\mathbf{f}^T \cdot \mathbf{x} \tag{1}$$

where $V_o(.)$ is the potential energy surface (PES) of a molecular system under consideration, or its free energy surface, under zero external force. $\mathbf{f}$ is the unit vector representing the direction of an external force acting on the molecule and F is the magnitude of the force. The superscript T indicates the transpose. Note that the force is a vector quantity, where both direction and magnitude are important. By $\mathbf{x}$ we represent the corresponding part of the molecule in arbitrary coordinates where curvilinear, internal coordinates are normally used. Note that they depend on the curvilinear metric [10] which we will ignore here. Equation (1) is the simplest possible equation, with a linear external force.

Under this force, the stationary points of the PES move. The new barrier of the effective PES changes, it is the sum of the differences

$$\Delta V = V_o(\mathbf{x}_{sp}) - V_o(\mathbf{x}_{min}) \text{ and } -F\,\mathbf{f}^T \cdot (\mathbf{x}_{sp} - \mathbf{x}_{min})\,. \tag{2}$$

$\mathbf{x}_{sp}$ and $\mathbf{x}_{min}$ are the transition state and ground state configurations, correspondingly. The two parts can play together or act against each other. This complicates the overall picture. The second part, $\Delta\mathbf{x} = \mathbf{x}_{sp} - \mathbf{x}_{min}$ in Eq. (2) has been discussed in Refs. 6, 11, for example. We will discuss the first summand below. Its solution curve is usually curvilinear.

To describe the motion of the stationary points, $\mathbf{x}_c$, the gradient of the effective PES for the stationary points, $V_f(\mathbf{x}_c)$, must be zero. This means that

$$\mathbf{g}(\mathbf{x}_c) = F\,\mathbf{f}\,, \tag{3}$$

where $\mathbf{g}$ is the gradient of the original PES. The value F changes as a non-linear parameter along the solution curve. At a new value, let us say F', a new point is found, $\mathbf{x}'_c$, such that Eq. (3) is satisfied for the new parameter value, F'. At each point $\mathbf{x}_c$ the parameter value, F, coincides with the square root of the gradient norm,

$$\left(\mathbf{g}^T(\mathbf{x}_c)\,\mathbf{g}(\mathbf{x}_c)\right)^{1/2},$$

if $\mathbf{f}$ is normalised. For the movement of any critical point, $\mathbf{x}_c$, we create a differential equation [2] as

$$\frac{d\mathbf{x}_c}{dt} = Det(\mathbf{H})\mathbf{H}^{-1}(\mathbf{x}_c)\,\mathbf{g}(\mathbf{x}_c) \tag{4}$$

where $\mathbf{H}^{-1}$ is the inverse of the Hessian matrix of the original PES, and $Det(\mathbf{H})$ is the determinant of this Hessian matrix. Variable t is the curve length parameter. Solutions of Eqs. (3) and (4) are called Newton trajectories (NTs). Equation (4) was created long ago by Branin [12] who used the so-called adjunct Hessian. It is the desingularized matrix $\mathbf{A} = Det(\mathbf{H})\,\mathbf{H}^{-1}$. Each solution of the Eqs. (3) and (4) to different directions, $\mathbf{f}$, connects a minimum with a saddle point (SP) of index one, SP_1. In chemistry this is called the transition state (TS). In general, an NT connects stationary points with an index difference of one [13–15]. A solution curve must pass through a point where

it holds $Det(\mathbf{H}) = 0$. The factor, $Det(\mathbf{H})$ in Eq. (4) desingularizes the equation [12]. The force in the direction $\mathbf{f}$ with the magnitude to reach the $Det(\mathbf{H}) = 0$ point forces the coalescence of the former minimum and the former saddle SP_1. This event is called the bond breaking point (BBP) [3]. In n dimensions, the $Det(\mathbf{H}) = 0$ manifold crosses the manifold of the valley-ridge inflection points (VRI) anywhere on the PES [14, 16–19] which play an important role in the theory of NT. On our 2-dimensional PES, a singular NT meets the VRI point. The singular NT forms the separatrix for NTs that may be an indicator of the catch-bond behaviour [4].

The paper is organised as follows. In the next Sect. 2 we report the chemical background of the model of the PES of the proposed tweezers model. Section 3 presents the mechanical model and first results with catch-bonds. We describe the catch-bond character of two quite different excitation directions based on NT theory, in particular, we find an example of so-called ideal bonds in Sect. 3.2. Finally we discuss the results in Sect. 4, and report conclusions based on the present model in Sect. 5. In an appendix we describe the calculation of NTs on a 2D PES.

2 The chemical background

Ligand-receptor interactions that are reinforced by mechanical stress, catch-bonds, play a major role in cell-cell adhesion [20]. The motivation for the tweezers design of Dansuk and Keten [1] is based on analyses and observations on the bacterial catch-bond protein FimH, a two-domain protein comprising a pilin domain and a lectin domain [21, 22]. The pattern is that of an allosteric reaction, compare Fig. 2 of References [6]. FimH proteins exist in an open conformation (PDB: 4XOD) and a closed conformation (PDB: 4XOB) of the ligand binding pocket, which are located on the lectin subunit [20]. The pilin domain connects FimH to bacterial appendages, while the lectin domain contains a binding pocket that facilitates the attachment of the adhesin to cell surface ligands [6, 23]. This two-domain structure is essential for allosteric reactions including the catch-bond formation, as the interactions between the lectin and pilin domains determine the conformational state and the ligand-binding properties of the lectin domain. The lectin binding pocket, along with its ligand-enclosing clamp loop segment, mediates the ligand affinity shown in Fig. 1. In the open conformation of the FimH-ligand complex, the loop segment interacts minimally with the ligand (Fig. 1A). Conversely, allosteric changes cause the loop to close around the ligand in the closed conformation, forming additional interactions (Fig. 1B). These allosteric changes result from mechanical tensile stress, which promotes domain separation and releases the lectin domain from the pilin domain (Fig. 1C, D). Although both conformations can bind to the ligand, the ligand remains bound longer in the closed conformation due to newly formed interactions [24]. It should be noted that the binding site and loop regions constitute a very small part of the whole protein. They are two 8-amino-acid residues on the 158-residue lectin domain.

The tweezers design mimics the essential characteristics of FimH which features two distinct conformational states; an open state with low affinity for its ligand, and a closed state with higher ligand affinity. The transition between these states is force-regulated by a switch, and increased ligand affinity in the closed state is achieved

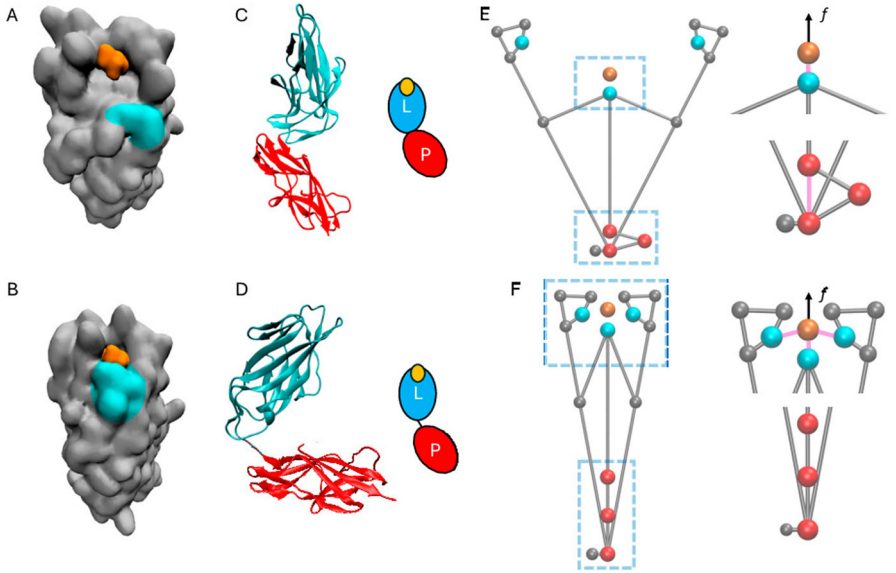

Fig. 1 FimH and tweezer design. **A**, **B** Lectin domain of FimH: the mannose ligand (orange) is bound to the ligand binding site in both the open and the closed conformations. **B** During the transition of FimH from its open to the closed conformation, the clamp loop segment (highlighted in cyan) closes on the ligand forming new interactions. **C**, **D** Open and closed conformations of the FimH protein with lectin (cyan) and pilin (red) domains, together with their schematic representation: Mechanical tensile stress promotes domain separation, leading to the release of the lectin domain from the pilin domain, consequently inducing allosteric changes in the binding sites. **E**, **F** The tweezer design, inspired by FimH, features primary and secondary binding sites (cyan) and a switch (red). In the open conformation (**E**), the ligand (orange bead) interacts with the tweezers, and the switch members are angled, held together by a pairwise interaction. In the closed conformation (**F**), the ligand forms three interactions with the tweezers, and the switch members align straight. Close-up views of the ligand binding site and the switch are provided on the right side of (**E, F**). Interactions and applied external forces are indicated by pink dashed lines and black arrows, respectively (Colour figure online)

through the formation of new interactions between the ligand and the tweezers. In the open conformation (Fig. 1E), the tweezers's arms are widely spaced, allowing the ligand (orange bead) easy access to the main binding site (MBS) at the centre of the binding pocket (central cyan bead). Secondary binding sites (SBS) are located on the arms of the tweezers (lateral cyan beads). SBS perform a function similar to that of the ligand-enclosing clamp loop segment found in the FimH protein. When the ligand is attached to the MBS (represented by the pink line in Fig. 1E) and the tweezers are in their open conformation, the ligand does not interact with the SBS, because they are positioned much farther apart. Conversely, in the closed conformation (Fig. 1F), the arms of the tweezers rotate towards the centre, enabling interactions between the ligand and the SBS. These new interactions (Fig. 1F, pink lines) stabilise the ligand and increase the adhesion energy, resulting in a higher ligand affinity in the closed conformation.

In order to facilitate force-dependent transitions between the two conformations, we incorporate a switch into the tweezers. This switch consists of a two-membered hinge

with a pairwise interaction between its two free ends (red beads in Fig. 1E, F). In the open conformation, the members are angled; however, when the pairwise interaction between the red beads is disrupted by external forces, the members straighten. A rigid member connects the switch to the MBS. Straightening the switch moves the MBS upward and drives the tweezers's arms inwards, leading to the closed conformation. Thus, the breaking and reforming of switch interactions control the transition between the conformations. This switch functions in a similar way to the interface between the lectin and pilin domains of FimH. Like the linkers in the domain interface, the tensile force promotes the separation and elongation of the protein, thus facilitating allosteric changes. Note that the masses of the MBS and the arms are kept small. The switch and the rigid linker loosely represent the larger mass of the rest of the protein.

One of the most prominent catch-bond behaviour has been reported for this protein FimH [25–27]. Although the tweezers are modelled after FimH, the design of the tweezers mirrors similar biphasic mechanisms observed in P-selectin and integrin proteins. Selectins, which are crucial for the binding of the white blood cells, exhibit two conformational states: a compact, inactive state with fewer accessible ligand-binding sites, and an elongated, active state with fully exposed and optimally oriented binding sites, which enhances interactions with ligands such as PSGL-1 [28]. Similarly, the $\alpha 5\beta 1$-integrin binding to fibronectin transitions from a bent to an extended conformation under force, revealing synergistic sites that stabilise the interaction [29].

The tweezer design offers a fundamental structural explanation for catch bond behavior. However, by analyzing our design through the lens of allostery, we can derive broader design principles that are applicable to other geometries. At first glance, the simplicity of the serial two-degree-of-freedom system, used below, with just two vibration modes, may not appear highly relevant to proteins. However, it can be argued that the "switch" functions similarly to a soft vibrational mode linked to low-frequency conformational dynamics, driven by large modal masses and low stiffness, while ligand interactions correspond to a high-frequency vibrational mode associated with a lightweight molecule tightly bound to a binding site. In fact, elastic networks exhibiting allostery typically have a soft region constrained by more rigid regions.

Another tweezer model is under discussion by the buckybowl buckycatcher model for fullerenes and other host-guest complexes [30–37]. These are more functional molecular capsules, cages and containers. None of these pincer studies test the behaviour of catch bonds. A slightly weaker model has been discussed by the 'lever-arm-effect' of a mechanical transformation in the diarylethenes [38–40].

3 The mechanical model

The model of Dansuk and Keten [1] and its coordinates are shown in Fig. 2. h is the length of the axis of the tweezer model, which starts at 16.25 Å and its final extension is 21.75Å and y is the dissociation coordinate of the dark yellow particle; its equilibrium number is $\sigma_{MBS} = 2$Å and its direction is given by the coordinate y in Figs. 2 and 4.

The MBS is the main bound state, whereas the SBS is a side bound state. They can be collective coordinates of the protein [27].

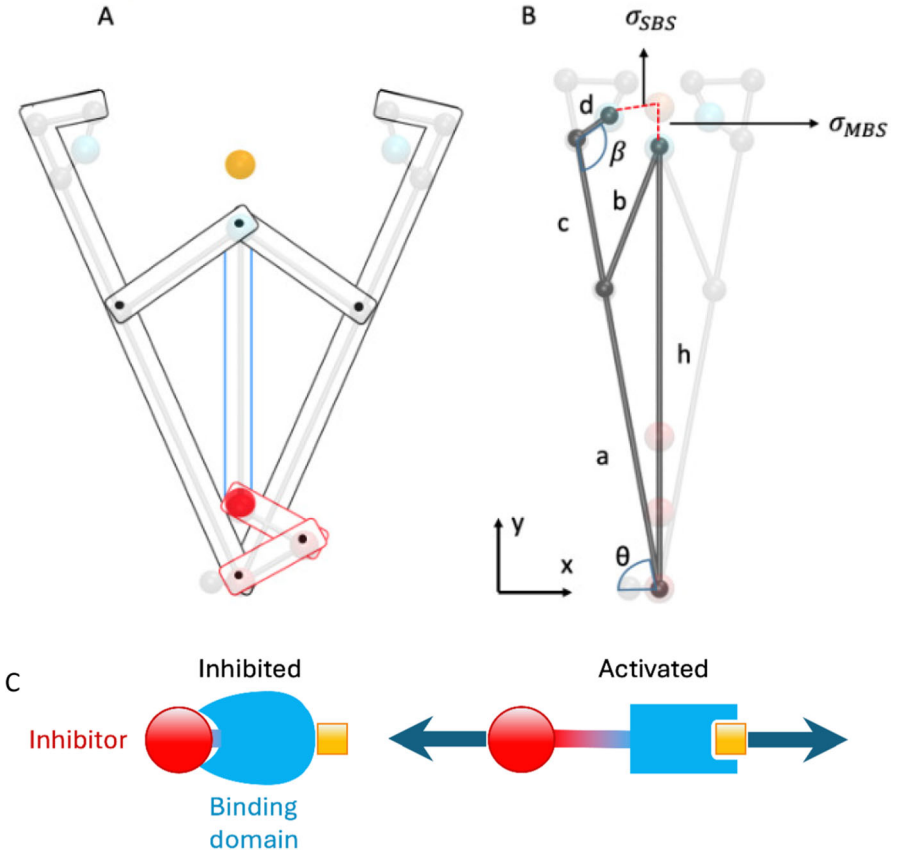

Fig. 2 **A** Mechanical tweezer model. **B** Coordinates used in the formulas. **C** Scheme of an allosteric tweezer model, see Ref. [6]

The used figures are: $a = 15$, $b = 7.5$, $c = 7.5$, $d = 2$, $h_o = 16.25$, all in Å, and $\beta = 114.5°$. The maximum length of $h_{max} = 22.5$. The model starts from the angle of the tweezers, see the supplementary material in Ref. [1].

$$\theta(h) = \arcsin\left[\frac{a^2 - b^2 + h^2}{2\,a\,h}\right] = \arcsin\left[\frac{168.75 + h^2}{30\,h}\right] \tag{5}$$

It is shown in Fig. 3.

The distances in $(x,\ y)$ system (see Fig. 2B) of the tweezer arm from the dark yellow atom are coordinates x_s and y_s.

$$x_s(h) = (a + c)\cos\theta(h) - d\cos(\beta - \theta(h)) = 22.5\cos\theta - 2\cos(1.997 - \theta) \tag{6}$$

$$y_s(h) = (a + c)\sin\theta(h) + d\sin(\beta - \theta(h)) = 22.5\sin\theta + 2\sin(1.997 - \theta) \tag{7}$$

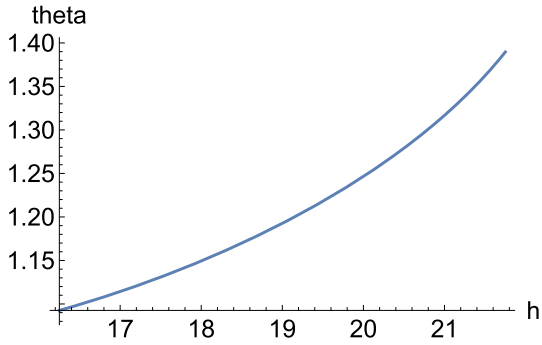

Fig. 3 Graph of angle θ in rad units

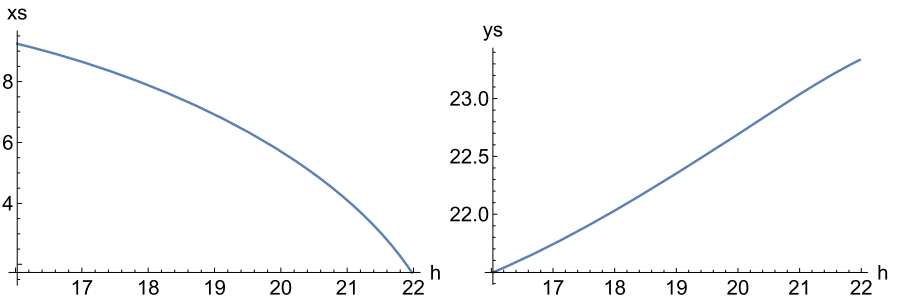

Fig. 4 Coordinates $(x_s,\ y_s)$ of the arm of the tweezers describe the distance from dark yellow atom which is at $h + y$ (Colour figure online)

($\beta = 114.5°$ corresponds to 1.997 rad.) They are shown in Fig. 4.

With the two Cartesian distances, one obtains the distance σ_{SBS} of Fig. 2 of the dark yellow atom from the tweezers, where

$$\sigma(h, y) = \sqrt{(y + h - y_s(h))^2 + x_s(h)^2}\ .$$

The index SBS is omitted in the following. The 2D form of the distance from the tip of the tweezers to the dark yellow atom is shown in Fig. 5A. The σ distance is used below in pc2.

The following Morse potential curves (pc) have been adopted from Dansuk and Keten [1]. with the parameters $D_1 = 5$, $\alpha_1 = 5$ and $\sigma_1 = 2$

$$pc1(y) = D_1(1 + Exp[-2\alpha_1(y - \sigma_1)) - 2Exp[-\alpha_1(y - \sigma_1)]) \tag{8}$$

D_1 is the dissociation energy of the bond in energy units kcal/mol, α_1 is the inverse width of the potential in 1/Å, and σ_1 is the equilibrium distance of the corresponding bond in Å. The plot of pc1 is shown in panel A of Fig. 6. The position $y = 2$ represents the minimum energy at level zero, regardless of the opening of the tweezers.

Each side arm develops a potential with $D_2 = 5$, $\alpha_2 = 8$ and $\sigma_2 = 4.46$

$$pc2(\sigma) = D_2(Exp[-2\alpha_2(\sigma - \sigma_2)] - 2Exp[-\alpha_2(\sigma - \sigma_2)]) \tag{9}$$

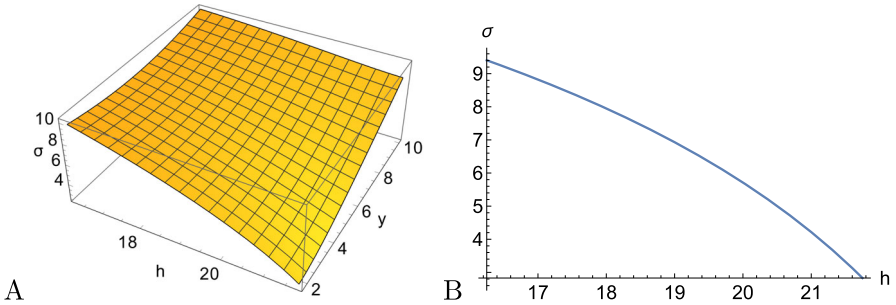

Fig. 5 **A** Image of distance surface $\sigma(h, y)$ of the arm of the tweezers from the dark yellow atom located at h+y. **B** Section of distance surface $\sigma(h, y)$ of the arm of the tweezers from dark yellow atom at y=2 (Colour figure online)

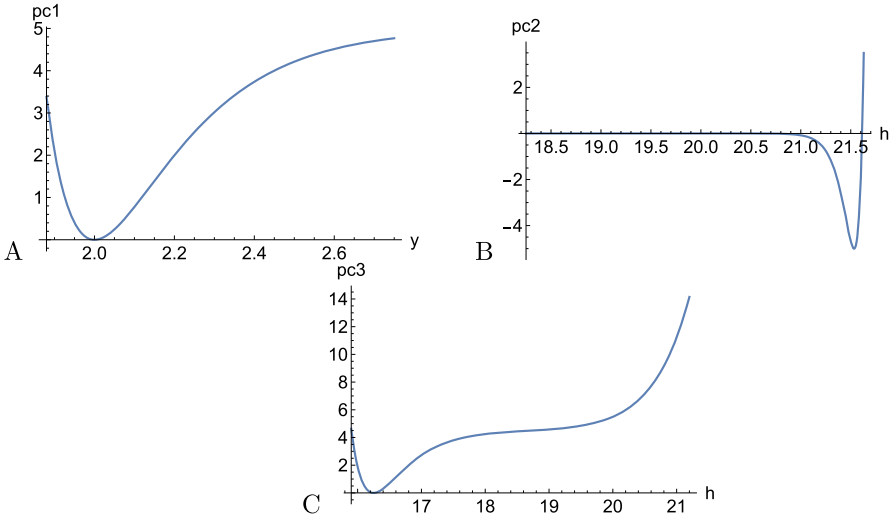

Fig. 6 Upper left panel (**A**) potential curve $pc1(y)$. **B** Morse potential of the tweezers which closes with increasing distance h. **C** Morse potential pc3 of the tweezers, for Eqs. (8) to (10), see text

Note that σ depends on y and h in a phytagorean form. This pc2-part starts at the zero level and gains energy to negative values for decreasing σ. A section of pc2 is shown in Fig. 6B. The complete PES is shown in Fig. 7. Note the missing summand 1 in the formula which describes the real gain of energy for the closing of the tweezers starting from a level close to zero.

The allosteric closing of the tweezers are modeled by a combination of the functions pc2 and pc3. Note that the result is the key-SP named TSz along the h-axis, in Figs. 8 and 9. For pc3 we again use a Morse potential approach, with the parameters

$D_3 = 4.5$, $\alpha_3 = 2$ and $\sigma_3 = 16.25$.

$$pc3(h) = (1 - h/10)^{20} + D_3\,(1 + Exp[-2\alpha_3(h - \sigma_3)] \\ -2\,Exp[-\alpha_3(h - \sigma_3)]) \tag{10}$$

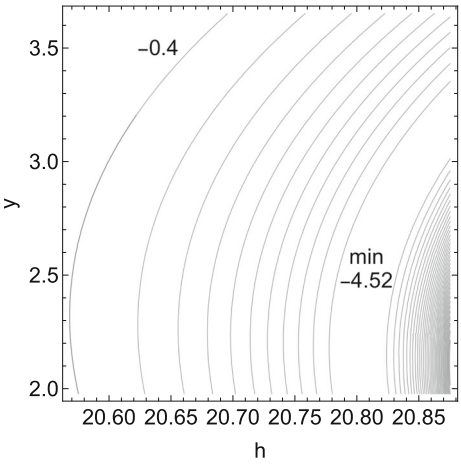

Fig. 7 2D version of the potential $pc2(\sigma(h, y))$

The profile pc3 is given in Fig. 6C. In addition, this potential starts at the zero level for the global minimum of the open tweezers, at $h = 16.25$. The artificially first part of formula (10) saves a strongly increasing potential at the high h edge to prevent the tweezers from overstretching the h-coordinate. Compare Fig. 8 with the deep valley on the right side for the closed tweezers, which is a result of this ansatz. The $\sigma_3 = 2$ given in Ref. [1] is changed here.

We use a factor of 2 for pc2 because of the two symmetric arms, left and right, of the tweezers. The sum formula for the PES is

$$V_o(h, y) = pc1(y) + pc3(h) + 2\ pc2(\sigma(h, y)) \tag{11}$$

with coordinates (h, y). The PES is shown in Fig. 8. This sum of four potentials for the tweezers for a model of FimH proteins is the natural way to combine the different parts of the molecule. The other coordinates are fixed. This approach is in a certain contrast to the current case of L-selectin with catch-bond behaviour, where the authors have used the product of two parts of 1D potentials [9]. Equation (11) is the main approach of this work. Its computation is done by the Mathematica program, version 13.3.1.0 for Linux x86(64-bit), as well as the computation of the inclusion of external forces by Eqs. (1) and (4). V_o in Eq. (11) means zero external force. Results for special forces are reported in Sects. 3.1 and 3.2. In an appendix we describe the calculation of NTs on a 2-dimensional PES section.

The thin lines in Fig. 8 are equipotential lines. The left minimum, M1, is stable for the 'open' tweezers, at $h = 16.25$ and $y = 2$. The dissociation direction is towards increasing y-coordinate, outside with a Morse level of 5 kcal/mol. The transition state is denoted as TSdi. The dashed NT points to the direction (1, 1) when we pull the dark yellow bead with the relation of the force 1 to 1 to the tweezers closing. The blue curve is the singular NT through a VRI point (it is found by trial and error), and the green curves are Det(**H**) = 0 lines. The magenta NT is in the pure h-direction, (1,0), while the red NT points in the y-direction, (0,1). Note that NTs describe the motion of

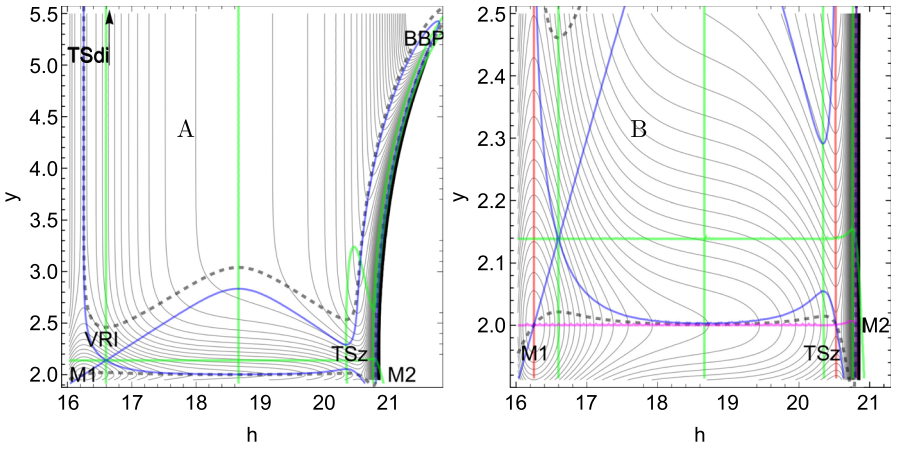

Fig. 8 **A** PES of the tweezers. **B** lower part enlarged, the level lines are different. Green are the Det(H) = 0 lines crossing the VRI points (Colour figure online)

stationary points under the corresponding force direction for an increasing magnitude of F.

Minimum M1 is at point $(16.25, 2)$ with energy 0, Minimum M2 is at point $(20.804, 2)$ with energy -0.8 kcal/mol, which is the global minimum, but the late TSz between them is at $(20.521, 2)$ with energy 6.86 kcal/mol, a slightly larger barrier than the dissociation at 5 units at TSdi. The symbol z in TSz means the 'zero-line' of the tweezers, at a distance of $y = 2$. Therefore the left minimum M1 is stable for an open tweezer. The minimum M2 on the right describes the closed tweezers. It is stable without an external force. However, a force is required to move the tweezers from the open to the closed form, given, for example, by the direction of the dashed NT. (One could also use a force only to close the tweezers (1,0) in the magenta colour; the NT is given in Fig. 8B.) The lower M2 then acts as a 'trap' trick for the catch-bonds [20].

The uphill left valley pathway undergoes a single dissociation of the dark yellow bead with the Morse level of TSdi at 5 kcal/mol for $y \to \infty$. The TSz between the minima is slightly higher, and there should not be a large probability of a 'spontaneous' movement of the tweezers into its closed form, compared to the probability of dissociation.

Figure 9 shows enlarged parts of the PES. Diagonal to the right emerges a ridge that should disappear somewhere on the slope. The NTs used there have turning points, and a final BBP is included in the upper right corner of Fig. 8A at $y = 5.6$.

If one excites the pure y-direction, along the force vector $(0, 1)$, then the left TSdi and the minimum M1 move together and finally coalesce. The barrier decreases during this time. Thus, the y-bond alone of an open tweezers exhibit a slip character.

One can also note, especially for Fig. 8B, that on the $y = 2$-line we find a quasi-shoulder of the PES at $(18.65, 2)$, a point with approximately zero curvature in the path direction, but which is not a minimum, nor TS, compare below Fig. 10. The dashed or magenta NTs indicate how the path from M1 to M2 can be increased by an external force.

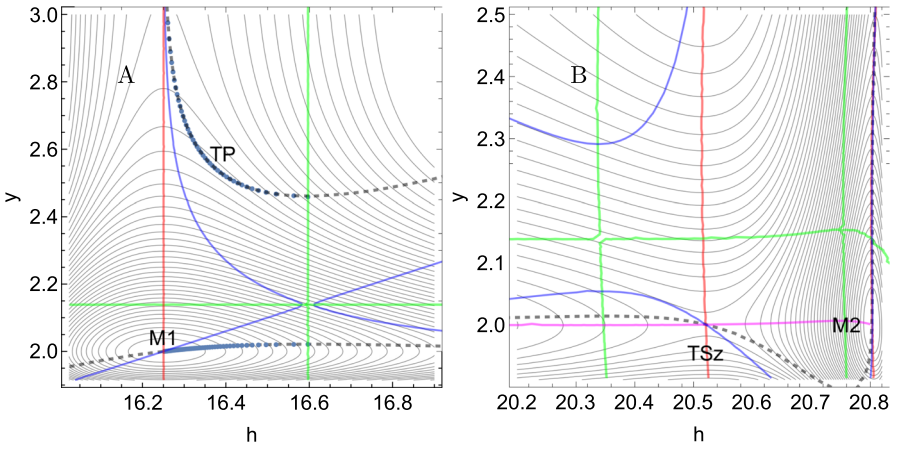

Fig. 9 **A** Left lower part of PES enlarged, TP is an 'inverse' turning point of the dashed NT. Dense blue dots are explicitly computed points of the dashed NT. **B** Right lower part of the PES enlarged (Colour figure online)

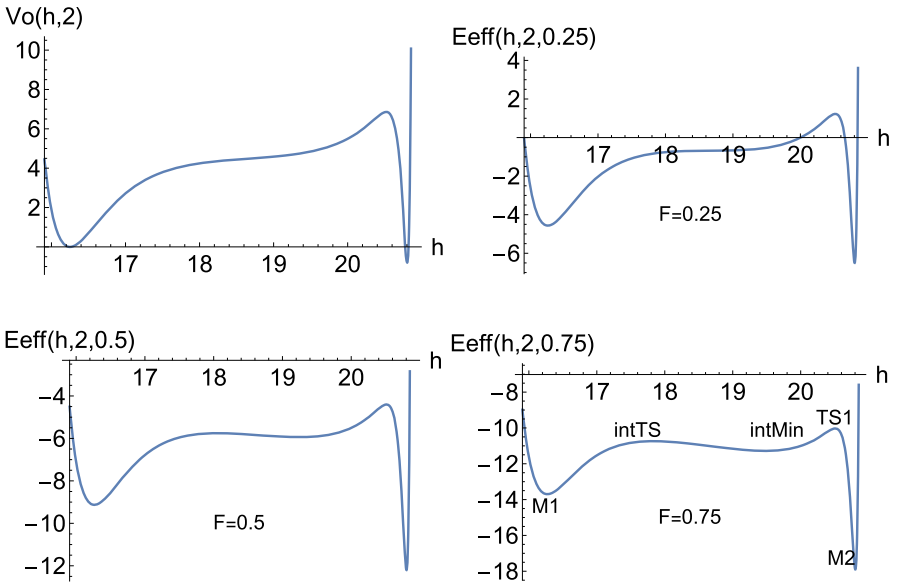

Fig. 10 Energy profile of a curve near to the minimum energy path (MEP) on the $y=2$ valley, for the dashed excitation, with F = 0 from left above, over F = 0.25, F = 0.5 to 0.75 right below

3.1 NT belonging to direction (1, 1)

We assume an excitation of the dark yellow bead by a force $(0, 1)$ of magnitude 1, but at the same time an excitation of the tweezers closing by a force $(1, 0)$ of 1. Under the dashed force NT, the moved minima follow the corresponding NT up to the TSs, and at a certain amount, the barriers disappear. Note that for simplicity we do not

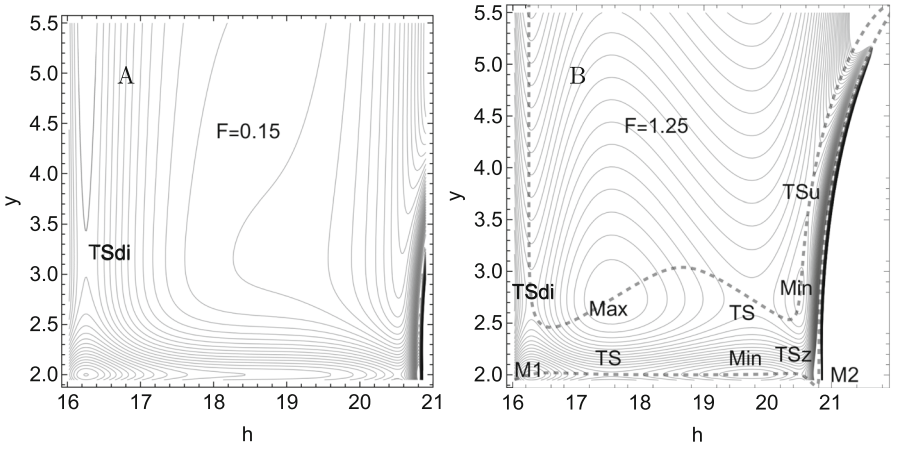

Fig. 11 **A** Effective PES for the dashed excitation, with F = 0.125 and **B** with F = 1.25 kcal/mol/Å. Here a new upper TSu appears near $y = 3.7$. The minimum M2 was before in a 'dead' valley on V_o

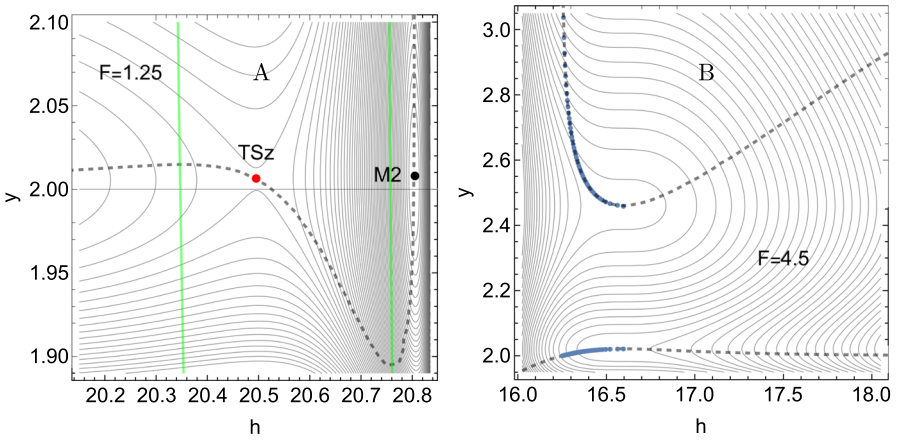

Fig. 12 **A** Enlargement of the right lower region around the TSz (red point) of Fig. 11B. M2 is at the black point. Both of the points are moved apart and are over their former $y = 2$-line. **B** NTs drawn on the effective PES for F = 4.5 kcal/mol/Å. Corresponding blue dots for different forces are used for the calculation of the barrier in Fig. 13A (Colour figure online)

normalise this direction $(1, 1)$ by $1/\sqrt{2}$, contrary to the definition in Eq. (1); all forces in this section are to be multiplied by $\sqrt{2}$.

The upper and lower branches of the dashed NT are separated by the VRI point, see Figs. 8 and 9. A singular NT (in blue) forms the separatrix for the dashed NT. The existence of a separatrix could be an indicator of catch-bond behaviour [4].

We still study the path from M1 to M2. Using the excitation along the direction $(1, 1)$ leads to a change in character from a valley with one TSz to one with two TSs, as shown in Fig. 10. It emerges as an intermediate minimum and an intermediate TS. One can also observe that the global character of the minimum M2 becomes stronger. Next we will follow this excitation along the dashed NT. In Fig. 11A, an excitation of

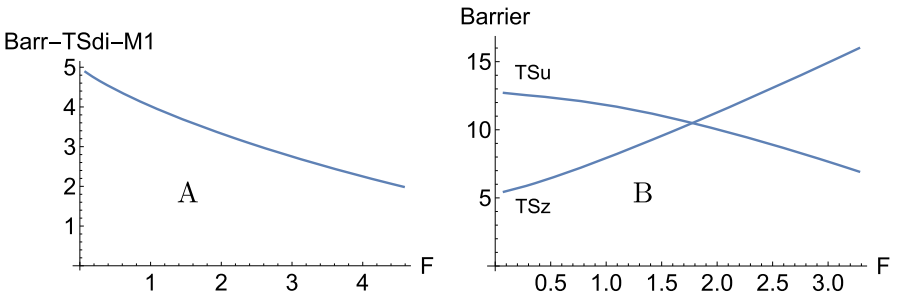

Fig. 13 **A** Barrier in kcal/mol between two paths along two branches of the dashed NT for the open tweezers of Fig. 12. The left axis is the barrier of TSdi to the minimum M1. The barrier does not disappear with increasing F. **B** Two barriers of the tweezers in kcal/mol: the increasing line is the barrier from M2 to TSz, the decreasing line is M2 to TSu

$F = 0.125$ kcal/mol/Å is applied. We observe a strong downward movement of the left dissociation TS (TSdi) to $y = 3.3$. In contrast, in Fig. 11B for $F = 1.25$, we observe many new weak stationary states: a new minimum and a new TS on the zero line $y = 2$, and on the dashed NT, a maximum at $(17.5, 2.7)$, a further TS at $(19.8, 2.7)$, a minimum at $(20.6, 2.75)$, and an next upper TSu at $(20.7, 3.75)$. However, these points still have high energies, so the main possible exchange takes place between TSdi and the two minima M1 and M2. In Fig. 11B an additional minimum 'Min' emerges on the path between M1 and TSz. Fig. 12A is an enlargement of the region around M2. More important here is the direction of the dashed NT across the TSz. Although the excitation $(1, 1)$ points to the 'north-east', the NT counterintuitively goes in the 'north-west' direction, and it almost holds the energy level of the TSz itself. However, minimum M2 moves in its deep vally towards 'north' and becomes deeper under the force. It moves away from TSz. The effect is, by comparison, the catch bond character in this direction of the dashed NT.

Such an explanation of catch bonds was proposed by Suzuki and Dudko [8] 15 years ago, by an orthogonal NT to the corresponding SP. Here the direction is only oblique to the valley path, and the effect of the excitation is only a slight catch bond character. Note that the dashed NT along the MEP M1 to M2 has no turning point (TP), both before and after TSz. Nevertheless, it shows a catch-bond behaviour. This is a new case in addition to the cases discussed in Ref. [4].

Another reason for the catch-bond character could be that the y coordinate does not change along the MEP from M1 to M2, but the h coordinate increases. And from the M2 minimum uphill, the movement increases the y coordinate but does not change the h coordinate. Here, the second part of Eq. (2) seems to play an additional role in the catch-bond character.

However, at higher force levels, the previously high TSu will become less energetic and become the main channel for dissociation from the minimum M2. Excitation along the dashed direction will decrease the left barrier, TSdi, and TSz is consistently higher, as shown in Figs. 11 and 13. The blue points on the NT in Fig. 12B are the calculated data for the barrier comparison. Under the force direction $(1, 1)$ there is then an intermediate maximum on the effective PES, shown in Figs. 11 and 15. Although

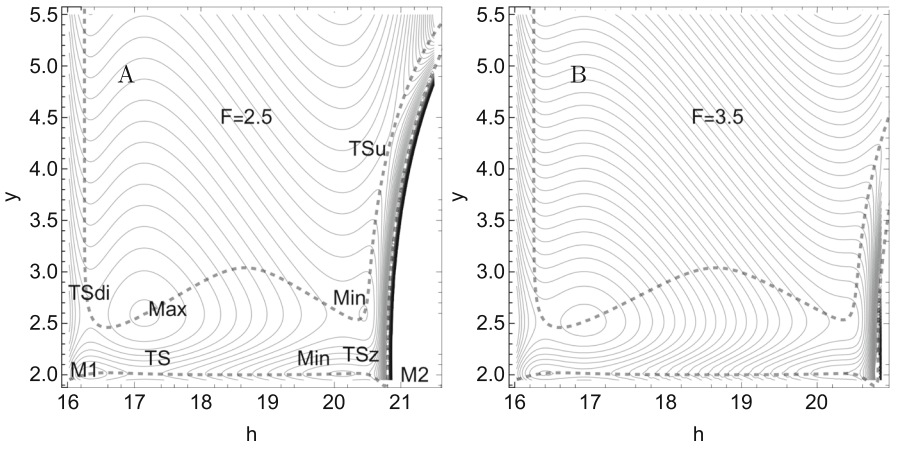

Fig. 14 **A** Effective PES for dashed excitation with F = 2.5 kcal/mol/Å. **B** Effective PES for dashed excitation with F = 3.5 kcal/mol/Å

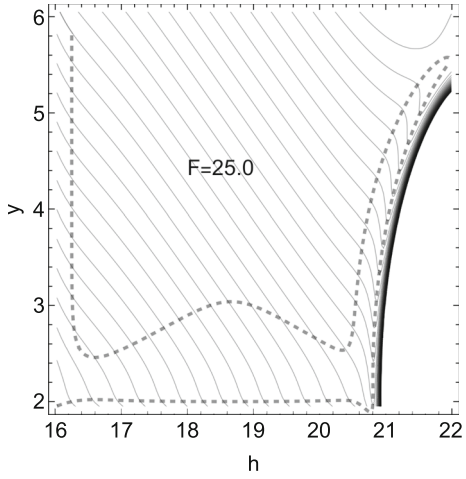

Fig. 15 Effective PES for the dashed directional excitation, with F = 25 kcal/mol/Å. All minima have disappeared. Only dissociation with increasing y takes place

the upper branch of the NT reaches the crest of the ridge of the PES, the difference decreases. Figure 13A shows the barrier height.

The tweezers are stable in their open form. However, if it is possible to excite a closure along the minimum energy path (MEP) along the h-axis then the closed form, M2, is deeper in energy than the open form, M1. This is a first catch-bond gap.

Starting from M2, the excitation along the dashed NT causes a catch-bond increase of the barrier TSz, as shown by the rising curve in Fig. 13B. This is the main result of this work. However, at $F > 1.8$ the energy difference between the global minimum, M2, and TSz becomes larger compared to the difference between M2 and TSu which becomes the lower barrier. In Fig. 13B, the first difference increases with F, it describes the catch-bond behaviour of the state at the M2 minimum.

At $F = 1.8$ the TSu becomes lower than the TSz. The relationship between TSu and M2 is the usual slip bond behaviour. In summary we have a minimal catch-bond

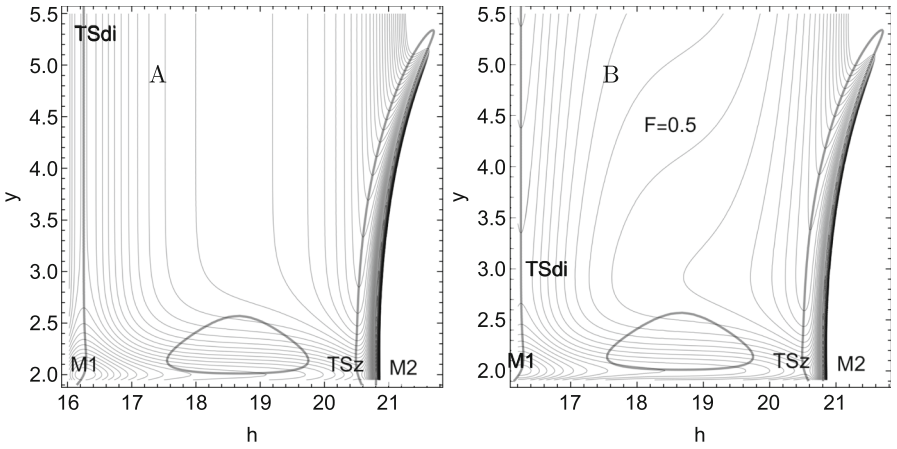

Fig. 16 **A** PES with the black NT to direction$(0.1, 1)$ for $F = 0$, and **B** for F$= 0.5$ kcal/mol/Å. The circular part of the NT begins at the shoulder and describes an emerging intermediate minimum and a new TS for increasing F

barrier of M2 to the TSz of the PES, but for $F > 1.8$ this is already finished. Note the small region of F values for the catch-bond behaviour, in contrast to Ref. [1]. In Fig. 14A, B one can follow this process. The two stationary points of Fig. 14A, Min and TS between TSu and Max, almost coalesce, and only quasi flat minimums remain in Fig. 14A. They disappear in Fig. 14B. So for $F = 2.5$ the upper TSu is lower that the left TSdi, but for $F = 3.5$, only the skew platform is over, and all structures are almost washed out. The minimum M2 exists above and moves 'uphill' in its former deep valley up to $F \approx 25$ kcal/mol/Å in the upper BBP (shown in the upper right corner of Fig.8A). This is demonstrated by the effective PES shown in Fig. 15.

3.2 NT belonging to direction (0.1, 1)—mechanical model for an ideal bond

We assume an excitation of the dark yellow bead by a force of 1 kcal/mol/Å, but at the same time a very small excitation of the tweezers closing by a force of 0.1 kcal/mol/Å. Under this force, we draw a thick black NT, as shown in Fig.16. Again, the moved minima follow the corresponding NTs up to their transition states, and at a certain value, the barriers disappear. Note that for simplicity we do not normalise this direction by $1/\sqrt{1.01}$.

The NT has a different characteristic. At saddle TSz, this NT crosses the saddle valley orthogonally, as opposed to the previous case where the dashed NT runs skew to the valley ground. The left and right branches of the black NT are separated by the VRI point. The separatrix is the same as in the previous subsection because it is the same PES. However through the flat minimum energy path of the connection from M1 to M2, forming a shoulder, we find a closed branch of the NT. Such a form is rare for NTs [41]. For the two deeper minima, M1 and M2, this has no significance.

If one starts an excitation at the minimum M1 along the given NT, then a simple dissociation takes place with a slip character. To argue with the given NT-direction,

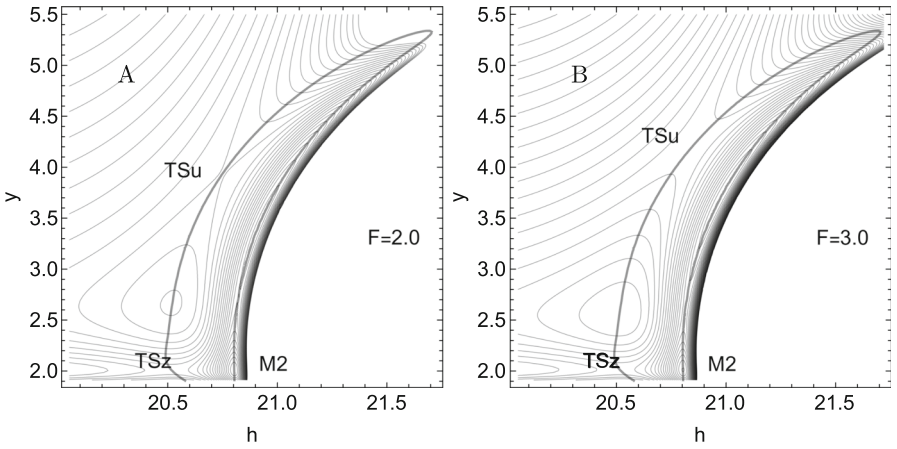

Fig. 17 **A** Effective PES for the excitation along the black NT, with first F = 2 and **B** with F = 3 kcal/mol/Å

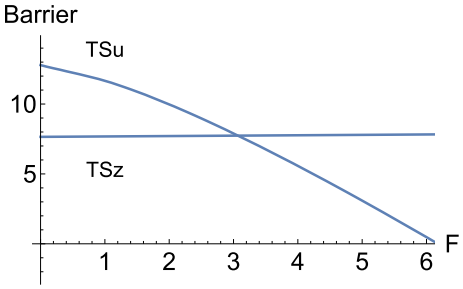

Fig. 18 Barriers in kcal/mol for the two different TSs, seen from M2, to TSz and TSu

we first move the tweezers in its closed form, by any other excitation. For example by the direction $(1, 0)$. Then we can assume that we start at the minimum M2. The lower M2 still causes a trap effect. Next, we will follow the excitation along the black NT with direction $(0.1, 1)$ starting at M2. In Fig. 17 one can observe that the new hill on the PES moves slightly to the right under excitation. At point (20.75, 3.75) another TSu appears on the ridge above. In Fig. 17B the TSu becomes lower than TSz (and TSdi, not shown).

The excitation of the tweezers in closed form, thus from the minimum M2, causes a catch-bond behaviour of the bond up to a value of $F = 3.1$. However, the barrier height becomes almost constant, and its increase is very small. Such a characteristic is called an 'ideal' bond [42, 43]. Note that the corresponding NT for this excitation is not the singular NT through a VRI point that marks the boundary, the separatrix, where catch-bonding can begin.

In Fig. 18 one can observe that the barrier height crosses with the upper TSu, again for $F \approx 3.1$ kcal/mol/Å. This upper TSu quickly becomes the dominant TS for dissociation in the y-direction.

4 Discussion

It is not exactly easy to come up with a theory of catch-bonding [4, 8, 9]. So we argue for our parameters: The dissociation level of pc1 should be low compared to pc3, but twice as high as pc2. Therefore, TSz under force should be slightly higher than the left TSdi of the single dissociation of the dark yellow bead. The barrier TSz between the minima is the most important criterion for the catch behaviour. However, TSz should also not be too high so that the molecule can still transfer from minimum M1 to M2. On the other hand, the the newly emerging upper TSu should be as high as possible. The parameters of pc1, pc2, and pc3 are balanced for mathematical reasons. This interpretation involves some degree of speculation, as all parameters are based on mathematical reasoning more than chemical considerations. However we assume that we have constructed a model for an allosteric process.

A previous step at the beginning of a pulling excitation could be the 'pulling' along the force directions $(1,0)$, or at least $(1,1)$ along the connecting NTs in the valley between M1 and M2. Then the molecule, or the tweezers, can jump in another direction $(0.1,1)$, or stay on $(1,1)$. The right-hand minimum M2 indicates that there is indeed a catch-bond behaviour which can be observed by the trap action of this lower minimum.

We underline that we do not address how the behaviour of the PES relates to lifetime versus force curves [44]. We only treat the height of the corresponding TS but do not use simulations or statistics of trajectories. This means that we avoid possible side effects of such methods. We also do not address the temperature sensitivity of the catch-bond behaviour. This should be done in future work.

5 Conclusion

By fine-tuning of the parameters of three Morse potentials used, which should model an allosteric process, we can observe a mild catch-bond character for single bonds in the given tweezer model. Additionally, we find an ideal bond for a changed pulling direction. We hope that the given example of a PES for a 'mechanical' model with chemical background can help to further unravel the mystery behind the catch-bonds, and the discussed model with a positive catch-bonding result can pave the way to other models. There are some interesting conceptual mechanical models for catch-bonds in Fig. 2 of Ref. [6], or Fig. 7 of Ref. [45] and Fig. 1 of Ref. [46]. The tweezers of this paper could, with good will, be assigned to cases *c* to *e* in Fig. 2 of Ref. [6] where for the unsymmetric cases *c* and *d* the symmetry of the two tweezer arms in Eq. (11) is to cut. However, the field of real catch-bond behaviour in biochemistry is even larger [47, 48]. Further studies are therefore warranted.

Appendix

2D Examples—representation of NTs

[49]

In 2D toy examples, NTs can easily be represented by a graphical rule. It applies in two dimensions that the orthogonal direction to the force direction

$$\mathbf{f} = (f_1, f_2) \text{ is unique the direction } \mathbf{f}^{\perp} = (-f_2, f_1).$$

Then condition (3) that $\mathbf{f} \parallel \mathbf{g}$ is the zero of the scalar product

$$\mathbf{g}\, \mathbf{f}^{\perp} = \mathbf{0}.$$

In Mathematica, one can represent the corresponding NT by

$$\begin{aligned} &ContourPlot[-g1[x, y]\, f2[x, y] + g2[x, y]\, f1[x, y], \{x, 0, 5\}, \{y, 0, 5\}, \\ &\quad ContourShading \to False, PlotPoints \to 30, \\ &\quad Contours \to \{0.0\}, ContourStyle \to \{Thickness[0.008], Dashed\}] \end{aligned}$$

Acknowledgements Financial support: Spanish Structures of Excellence María de Maeztu program, through Grant No. CEX2021-001202-M; Agència de Gestió d'Ajuts Universitaris i de Recerca of Generalitat de Catalunya, Projecte:2021 SGR 00354.

Author contributions All authors contributed and reviewed the manuscript.

Funding Open Access funding enabled and organized by Projekt DEAL.

Data availability Data can be obtained by WQ. No datasets were generated or analysed during the current study.

Declarations

Conflict of interest The authors declare that they have no conflicts of interest, no affiliations with or involvement in any organization or entity with any financial interest in the subject matter or materials discussed in this manuscript.

Methods We used Mathematica 13.3.1.0 for Linux x86(64-bit) in the calculations. and in the representation of the figures. Compare the calculations of NTs using the Wolfram Mma-page: https://community.wolfram.com/groups/-/m/t/3167380.

References

1. K.C. Dansuk, S. Keten, A simple mechanical model for synthetic catch bonds. Matter **1**(2), 911–925 (2019)
2. W. Quapp, J.M. Bofill, Reaction rates in a theory of mechanochemical pathways. J. Comput. Chem. **37**, 2467–2478 (2016)
3. W. Quapp, J.M. Bofill, J. Ribas-Ariño, Analysis of the acting forces in a theory of catalysis and mechanochemistry. J. Phys. Chem. A **121**, 2820–2838 (2017)
4. W. Quapp, J.M. Bofill, Theory and examples of catch bonds. J. Phys. Chem. B **128**, 4097–4110 (2024)
5. M. Dembo, D.C. Torney, D. Hammer, The reaction-limited kinetics of membrane-to-surface adhesion and detachment. Proc. R. Soc. Lond. B Biol. Sci. **234**, 55–83 (1988)
6. W.E. Thomas, V. Vogel, E. Sokurenko, Biophysics of catch bonds. Annu. Rev. Biophys. **37**, 399–416 (2008)
7. A.V. Belyaev, I.V. Fedotova, Molecular mechanisms of catch bonds and their implications for platelet hemostasis. Biophys. Rev. **15**, 1233–1256 (2023)
8. Y. Suzuki, O.K. Dudko, Single-molecule rupture dynamics on multidimensional landscapes. Phys. Rev. Lett. **104**, 048101 (2010)
9. C.O. Barkan, R.F. Bruinsma, Topology of molecular deformations induces triphasic catch bonding in selectin-ligand bonds. Proc. Natl Acad. Sci. U.S.A. **121**, 2315866121 (2024)
10. W. Quapp, D. Heidrich, Analysis of the concept of minimum energy path on the potential energy surface of chemically reacting systems. Theor. Chim. Acta **66**, 245–260 (1984)
11. E. Evans, K. Ritchie, Dynamic strength of molecular adhesion bonds. Biophys. J. **72**, 1541–1555 (1997)
12. F.H. Branin, Widely convergent methods for finding multiple solutions of simultaneous nonlinear equations. IBM J. Res. Dev. **16**, 504–522 (1972)
13. W. Quapp, M. Hirsch, O. Imig, D. Heidrich, Searching for saddle points of potential energy surfaces by following a reduced gradient. J. Comput. Chem. **19**, 1087–1100 (1998)
14. W. Quapp, M. Hirsch, D. Heidrich, Bifurcation of reaction pathways: the set of valley ridge inflection points of a simple three-dimensional potential energy surface. Theor. Chem. Acc. **100**(5/6), 285–299 (1998)
15. M. Hirsch, W. Quapp, The reaction pathway of a potential energy surface as curve with induced tangent. Chem. Phys. Lett. **395**(1–3), 150–156 (2004)
16. M. Hirsch, W. Quapp, D. Heidrich, The set of valley-ridge inflection points on the potential energy surface of water. Phys. Chem. Chem. Phys. **1**, 5291–5299 (1999)
17. W. Quapp, M. Hirsch, D. Heidrich, An approch to reaction path branching using valley-ridge-inflection points of potential energy surfaces. Theor. Chem. Acc. **112**, 40–51 (2004)
18. W. Quapp, Can we understand the branching of reaction valleys for more than two degrees of freedom? J. Math. Chem. **54**, 137–148 (2015)
19. V.J. García-Garrido, S. Wiggins, The dynamical significance of valley-ridge inflection points. Chem. Phys. Lett. **781**, 138970 (2021)
20. M.M. Sauer, R.P. Jakob, J. Eras, S. Baday, D. Eris, G. Navarra, S. Berneche, B. Ernst, T. Maier, R. Glockshuber, Catchbond mechanism of the bacterial adhesin FimH. Nat. Commun. **7**, 10738 (2016)
21. W.E. Thomas, M. Forero, O. Yakovenko, L. Nilsson, P. Vicini, E. Trintchina, E.V. Sokurenko, V. Vogel, Catch-bond model derived from allostery explains force-activated bacterial adhesion. Biophys. J. **90**, 753–764 (2006)
22. G. Stirnemann, Recent advances and emerging challenges in the molecular modeling of mechanobiological processes. J. Phys. Chem. B **126**, 1365–1374 (2022)
23. I. Le Trong, P. Aprikian, B.A. Kidd, M. Forero-Shelton, V. Tchesnokova, P. Rajagopal, V. Rodriguez, G. Interlandi, R. Klevit, V. Vogel, R.E. Stenkamp, E.V. Sokurenko, W.E. Thomas, Structural basis for mechanical force regulation of the adhesin FimH via finger trap-like β sheet twisting. Cell **141**, 645–655 (2010)

24. E.V. Sokurenko, V. Vogel, W.E. Thomas, Catch-bond mechanism of force-enhanced adhesion: counterintuitive, elusive, but ... widespread? Cell Host Microbe **4**, 314–323 (2008)
25. J. Liu, L.A. Nunes Amaral, S. Keten, Conformational stability of the bacterial adhesin, FimH, with an inactivating mutation. Proteins **89**, 276–288 (2021)
26. W.E. Thomas, L. Carlucci, O. Yakovenko, G. Interlandi, I.L. Trong, P. Aprikian, P. Magala, L. Larson, Y. Sledneva, V. Tchesnokova, R.E. Stenkamp, E.V. Sokurenko, Recombinant FIMH adhesin demonstrates how the allosteric catch bond mechanism can support fast and strong bacterial attachment in the absence of shear. J. Mol. Biol. **434**, 167681 (2022)
27. O. Languin-Cattoën, F. Sterpone, G. Stirnemann, Binding site plasticity regulation of the FimH catch-bond mechanism. BioPhys. J. **122**, 2744–2756 (2023)
28. E. Evans, A. Leung, H. Volkmar, C. Zhu, Mechanical switching and coupling between two dissociation pathways in a P-selectin adhesion bond. Proc. Natl Acad. Sci. U.S.A. **101**, 11281–11286 (2004)
29. F. Kong, A.J. García, A.P. Mould, M.J. Humphries, C. Zhu, Demonstration of catch bonds between an integrin and its ligand. J. Cell Biol. **185**, 1275–1284 (2009)
30. Y. Zhao, D.G. Truhlar, Computational characterization and modeling of buckyball tweezers: density functional study of concave-convex $\pi - \pi$ interactions. Phys. Chem. Chem. Phys. **10**, 2813–2818 (2008)
31. C. Mück-Lichtenfeld, S. Grimme, L. Kobryn, A. Sygula, Inclusion complexes of bucky-catcher with c60 and c70. Phys. Chem. Chem. Phys. **12**, 7091 (2010)
32. S. Grimme, Supramolecular binding thermodynamics by dispersion-corrected density functional theory. Chem. Eur. J. **18**, 9955–9964 (2012)
33. R. Sure, S. Grimme, Comprehensive benchmark of association (free) energies of realistic host-guest complexes. J. Chem. Theory Comput. **11**, 3785–3801 (2015)
34. F. Menezes, G.M. Popowicz, How to catch the ball: Fullerene binding to the corannulene pincer. Molecules **27**, 3838 (2022)
35. B. Scholz, A.S. Oshchepkov, O. Papaianina, C. Ruppenstein, V.A. Akhmetov, D.I. Sharapa, K.Y. Amsharov, M.E. Pérez-Ojeda, An indacenopicene-based buckybowl catcher for recognition of fullerenes. Chem. Eur. J. **29**, 202302778 (2023)
36. A.S. Oshchepkov, Buckybowl molecular tweezers for recognition of fullerenes. ChemPhysChem **2024**, 202400435 (2024)
37. C.J.T. Cox, J. Hale, P. Molinska, J.E.M. Lewis, Supramolecular and molecular capsules, cages and containers. Chem. Soc. Rev. **53**, 10380–10408 (2024)
38. H.M. Klukovich, T.B. Kouznetsova, Z.S. Kean, J.M. Lenhardt, S.L. Craig, A backbone lever-arm effect enhances polymer mechanochemistry. Nat. Chem. **5**, 110 (2013)
39. R. Boulatov, Demonstrated leverage. Nat. Chem. **5**, 84 (2013)
40. C. Zhang, T.B. Kouznetsova, B. Zhu, L. Sweeney, M. Lancer, I. Gitsov, S.L. Craig, X. Hu, Advancing the mechanosensitivity of atropisomeric diarylethene mechanophores through a lever-arm effect. J. Am. Chem. Soc. **147**(3), 2502–2509 (2024)
41. W. Quapp, J.M. Bofill, M. Caballero, Search for conical intersection points (CI) by Newton trajectories. Chem. Phys. Lett. **541**, 122–127 (2012)
42. S. Rakshit, Y. Zhang, K. Manibog, O. Shafraz, S. Sivasankar, Ideal, catch, and slip bonds in cadherin adhesion. Proc. Natl Acad. Sci. U.S.A. **109**, 18815–18820 (2012)
43. S. Rakshit, S. Sivasankar, Biomechanics of cell adhesion: how force regulates the lifetime of adhesive bonds at the single molecule level. Phys. Chem. Chem. Phys. **16**, 2211–2223 (2014)
44. E.A. Novikova, C. Storm, Evolving roles and dynamics for catch and slip bonds during adhesion cluster maturation. Phys. Rev. E **103**, 032402 (2021)
45. R.P. McEver, C. Zhu, Rolling cell adhesion. Annu. Rev. Cell Dev. Biol. **26**, 363 (2010)
46. S. Adhikari, J. Moran, C. Weddle, M. Hinczewski, Unraveling the mechanism of the cadherin-catenin-actin catch bond. PLoS Computat. Biol. **14**, 1006399 (2018)
47. J. Nair, S. Chandel, M.K. Mitra, S. Muhuri, A. Chaudhuri, Effect of catch bonding on transport of cellular cargo by dynein motors. Phys. Rev. E **94**, 032403 (2016)
48. X. Guan, Y. Bian, Z. Guo, J. Zhang, Y. Cao, W. Li, W. Wang, Bidirectional allostery mechanism in catch-bond formation of CD44 mediated cell adhesion. J. Phys. Chem. Lett. **15**, 10786–10794 (2024)
49. M. Hirsch, Zum Reaktionswegcharakter von Newtontrajektorien. Dissertation, University Leipzig, Faculty of Chemistry and Mineralogy (2004)